

# High Through-Thickness Thermal Conductivity Composites Based on Three-Dimensional Woven Fiber Architectures

Keith Sharp\* and Alexander E. Bogdanovich†

3TEX, Inc., Cary, North Carolina 27511

and

Wenzhong Tang,‡ Dirk Heider,§ Suresh Advani,¶ and Michael Glowiana‡

University of Delaware, Newark, Delaware 19716

DOI: 10.2514/1.38108

Composites based on laminates of uniaxial or biaxial fiber reinforcements exhibit low through-thickness thermal conductivity, due to low matrix thermal conductivity and the number of interfaces in the thermal path. For applications near heat-generating components, the use of laminate composites in the surrounding structure can be limited by this inability to transport heat through the thickness. Three-dimensional orthogonal weaving provides an efficient, cost-effective method of placing high thermal conductivity yarns in the through-thickness  $Z$  direction of a preform to yield structural composites with high through-thickness thermal conductivity and with in-plane strength or stiffness comparable to laminates. Three basic research efforts investigated the efficacy of this approach: 1) weaving trials to determine the ability to three-dimensional orthogonal weave pitch carbon fibers and plied copper wires in the  $Z$  direction of the preforms, 2) through-thickness thermal conductivity testing of composites based on three-dimensional preforms, and 3) thermal modeling to describe several of the phenomena observed during thermal conductivity tests. During the testing, composites based on the three-dimensional orthogonal preforms with  $Z$  fiber volume fractions of only 5.5% measured a 12-fold increase in through-thickness thermal conductivity over a laminate composite, 8.4 versus 0.7 W/m K.

## Nomenclature

$H$	=	height of sample
$k$	=	thermal conductivity
$q_i$	=	heat flow at specified position
$R_{\text{int}}$	=	thermal resistance of interface
$T_i$	=	temperature at specified position
$V_f$	=	volume fraction
$V_{fz}$	=	volume fraction in the $Z$ direction
$z_i$	=	vertical position of thermistors
$\Delta z$	=	distance between thermistors

## I. Introduction

THE use of high conductivity fibers can result in high in-plane thermal conductivity of laminated or unidirectional composites, however, laminate composites exhibit low thermal or electrical conductivity in the direction perpendicular to the direction of the fibers. This limits their use near heat-generating elements, such as engines, gearboxes, pumps, or areas of heavy electrical loads due to their inability to transport heat to an external surface.

For the in-plane thermal conductivity of laminated and unidirectional composites, the parallel circuit analogy is well accepted in the composite literature and leads to a rule-of-mixtures (ROM) relationship summing the products of the volume fractions and thermal conductivities of the fibers and of the matrix. For the through-thickness direction, models of a more complex nature have been developed [1–9]. The heat flow through the thickness of laminated and unidirectional composites must traverse polymer-rich interlaminar regions with relatively low thermal conductivity, as well as pass through several fiber–matrix interfaces, each with an attendant restriction to the heat flow. Though none of the through-thickness models have proven completely accurate, all of the models show, and experiments confirm, that the through-thickness thermal conductivities are closer to the thermal conductivity of the matrix than that of the fibers. Thus, current composite technologies do not provide structural composites with high through-thickness thermal conductivity. As an example, a uniaxial composite of K1100 pitch carbon fibers (950–1100 W/m K) in an epoxy matrix (0.2 W/m K) can provide 595 W/m K in the direction of the fibers, while only measuring 1 W/m K perpendicular to them [10]. In 2-D laminated composites, parts based on a plain weave prepreg of YS-90 pitch carbon fibers (500 W/m K) in epoxy matrix measured 145 W/m K along the warp  $x$  and fill  $y$  directions, but only 1.0 W/m K through the thickness [11]. Loading the matrix resin with particulate can provide some increase in the through-thickness thermal conductivity, but the overall influence is limited and it comes at the cost of both lowering the mechanical properties of the resin [12] and increasing the fabrication complexity of the composite. In high-end applications, such as space radiators, high through-thickness thermal conductivity is achieved by making a carbon–carbon (C–C) composite and partially graphitizing the carbon matrix, resulting in through-thickness thermal conductivities in the range of 20–50 W/m K [10,13]. Again, this processing is expensive and the C–C composites are not suitable as structural members.

By placing high thermal conductivity yarns in the through-thickness  $Z$  direction of an orthogonal 3-D woven preform, structural composites with high through-thickness thermal conductivity can be manufactured with in-plane strength or stiffness comparable to

Presented as Paper 1870 at the 49th AIAA/ASME/ASCE/AHS/ASC Structures, Structural Dynamics, and Materials Conference, Schaumburg, IL, 7–10 April 2008; received 17 April 2008; revision received 24 July 2008; accepted for publication 24 July 2008. Copyright © 2008 by 3TEX, Inc.. Published by the American Institute of Aeronautics and Astronautics, Inc., with permission. Copies of this paper may be made for personal or internal use, on condition that the copier pay the \$10.00 per-copy fee to the Copyright Clearance Center, Inc., 222 Rosewood Drive, Danvers, MA 01923; include the code 0001-1452/08 \$10.00 in correspondence with the CCC.

\*Senior Research Engineer, 109 MacKenan Drive. AIAA Member.

†Vice-President Research and Development, 109 MacKenan Drive. AIAA Member.

‡Graduate Student, Center for Composite Materials, 213 South Academy Street.

§Assistant Director, Center for Composite Materials, 213 South Academy Street.

¶Associate Director, Center for Composite Materials, 213 South Academy Street.

traditional laminates. Costs can be kept low by the relatively small fiber volume fraction of potentially expensive yarns used in the Z direction. To demonstrate the efficacy of this approach, a variety of composites based on 3-D woven architectures were manufactured and their through-thickness thermal conductivities measured. Thermal modeling was used to better understand the thermal performance of the overall composite systems.

## II. Three-Dimensional Weaving and High-Conductivity Z Yarns

### A. Three-Dimensional Weaving

In orthogonal 3-D weaves, the through-thickness fibers are perpendicular to the plane of the fabric, as shown in Fig. 1. The fabric is held together with the Z (through-thickness) fibers. Using the multirapier process, such as that invented by the North Carolina State University College of Textiles [14] and further developed by 3TEX [15], all layers are simultaneously inserted in a single machine cycle. Thus, composites based on orthogonal 3-D woven preforms manufactured by this process compare favorably in cost to hand-laid 2-D laminates, especially as the number of layers increases.

The warp  $x$  yarns do not bend; they only advance linearly with each machine cycle. The weft  $y$  yarns lay flat through the fabric, then bend only outside the edge of the fabric. The Z yarns, in contrast, wrap around the top or bottom fill yarns during each fill yarn insertion to form a relatively small radius. The ability of Z yarns to withstand this bending, in turn, limits the fill yarn spacing in the final fabric. In the resultant fiber architecture, the warp and fill yarns are not crimped and the Z yarns remain approximately vertical with respect to the plane of the fabric. At low Z fiber volume fractions, the lack of crimp in the orthogonal 3-D architecture compensates for the small loss of in-plane fiber volume fraction, so that composites based on such preforms achieve equivalent or slightly greater in-plane strength and stiffness as a 2-D laminate with similar fiber volume fraction [16].

### B. Three-Dimensional Orthogonal Preforms with High Thermal Conductivity

Two materials appear to be the most desirable for placement in the Z direction to achieve high thermal conductivity—pitch carbon yarns and plied copper wires. Pitch fibers have both high thermal conductivity, some higher than copper's 398 W/m K, and light weight, on the order of 2.1 g/cm<sup>3</sup> compared to aluminum's 2.7 g/cm<sup>3</sup>. However, pitch carbon yarns have high modulus and are very brittle, limiting their ability to be 3-D woven in the Z yarn position, due to the large internal stresses generated as the Z yarn loops out of the surface and returns through the fabric. The other desirable material for thermal conductivity is copper, here in the form of thin-gauge copper wires, plied together to achieve the desired cross section, yet retain the needed flexibility. Copper has high thermal conductivity, good formability, and low cost, but adds weight with its density of 8.98 g/cm<sup>3</sup>. Further, for multifunctional materials, copper also provides high electrical conductivity, useful in

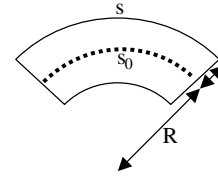


Fig. 2 Simple, single-fiber model for critical bend radius.

antistatic, electromagnetic interference, and lightning strike protection.

Bending the fibers in a yarn or the wires in a group of plied wires beyond a minimum radius will cause brittle fracture [17] or plastic deformation, depending on the fiber type. A schematic for a simple model for the bend radius of a single fiber is shown in Fig. 2. The minimum bend radius can be estimated by a simple model [18], described in Eqs. (1) and (2):

$$\varepsilon = \frac{s - s_0}{s} = \frac{r}{R + r} \quad (1)$$

$$R_c = \frac{r}{2} \left[ \frac{E}{\sigma_c} - 1 \right] \quad (2)$$

where  $\varepsilon$  is strain,  $s$  is the arc length of the outside of the fiber,  $s_0$  is the arc length of the center of the bent fiber,  $r$  is the fiber radius, and  $R$  is the bend radius.  $R_c$  defines the minimum radius the fiber can reach during preform manufacture without fracture or yielding. To use Eq. (2), fiber modulus  $E$  and critical stress  $\sigma_c$ , defined as the ultimate tensile strength for brittle fibers or as the tensile yield strength for elastic-plastic fibers, need to be determined.

Though it is useful as a guide, the simple model single-fiber  $R_c$  only partially explains the limitations imposed on weaving yarn bundles. Fibers in a yarn may vary in strength, in part due to surface damage accumulated during processing, such as winding onto spools. Other factors also influencing the ability to weave a fiber include sizing, anisotropy in the fiber's mechanical properties, the ability of the fibers to withstand abrasion, the yarn's friction, or the yarn's tendency to fray. Each of these factors further limits the formation of fabric preforms made from the high-modulus fibers. Thus, this simple model describes only a lower bound for radii in the fiber architecture.

Table 1 lists commercial pitch yarns, their properties and commercial prices, all ranked with respect to the thermal conductivity along the fibers. Also included in Table 1 is a measure of the cost effectiveness of the fibers as cost/unit of thermal conductivity.

In previous research [16], a series of 3-D weaving trials were performed to determine the ability to manufacture 3-D orthogonal woven fabrics with pitch carbon yarns in the Z yarn position. With a base fiber architecture consisting of two warp layers of T300 12k carbon fibers spaced at 4.7 ends per cm (12 dpi) and three fill layers of T300 6k carbon fibers, preforms were made with increasing fill yarn spacing until the Z yarns bending at the surface began to fail in brittle fracture. Once the maximum fill yarn spacing was determined, the same fiber type was tested in the fill direction to ensure that it could be used as a fill yarn during the weaving process. Because the warp yarns are bent the least, only yarns that failed when used in the fill direction were subjected to further trials in which they were used in warp yarn positions. These trials found Granoc YS-80 pitch carbon yarns as the optimum pitch carbon yarn for Z position and Granoc YS-95 for the warp and fill positions when high in-plane thermal conductivity is desired. Tests with Granoc YS90 and Mitsubishi K13C2U in the Z yarn position were unsuccessful, however, the yarns could be woven in the warp or fill directions. The Cytec K1100 and the Mitsubishi K13D2U yarns were not weavable in a 3-D orthogonal architecture, failing during the beat-up phase of weaving, even when input as warp yarns. In general, the tests on the Granoc yarns demonstrated a minimum bend radius that was 2.1–2.8 times over that predicted by the simple model.

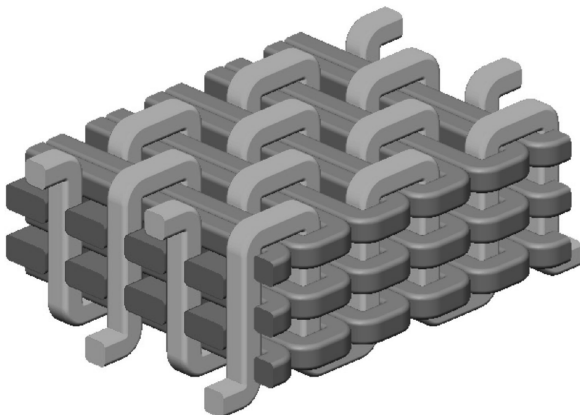


Fig. 1 Orthogonal 3-D weave.

**Table 1** Commercially available pitch carbon yarns

		Tow, k	Tensile modulus, GPa	Tensile strength, MPa	Thermal conductivity, W/m K	Density, g/cm <sup>3</sup>	Price, \$/lb	Cost per conductivity unit, \$/(W/mK)
Cytec	K-1100	2	965	3100	950	2.2	\$1500	\$1.58
Mitsubishi	K13D2U	2	935	3700	800	2.21	\$925	\$1.16
Cytec	P120	2	827	2410	640	2.18	\$600	\$0.94
Mitsubishi	K13C2U	2	900	3800	620	2.2	\$700	\$1.13
Nippon	YS-95A	1.5, 3, 6	900	3530	600	2.2	\$440	\$0.73
Nippon	CN-90	6	860	3100	500	2.21	\$200	\$0.40
Nippon	YS-90A	1, 5, 3, 6	880	3530	500	2.19	\$490	\$0.98
Nippon	CN-80	3, 6	780	3430	320	2.17	\$125	\$0.39
Nippon	YS-80A	1, 3, 6	785	3630	320	2.17	\$460	\$1.44
AL 6061			70	276	160	2.7	\$20	\$0.13

Ten 34-gauge soft annealed copper wires were plied into yarns for use in the Z yarn position and tested in similar 3-D weaving trials. The trials found that the plastic deformation of the copper wires did not limit the fill yarn spacing.

### III. Through-Thickness Thermal Conductivity Test Setup

#### A. Choice of Test Method

Two common methods for measuring the thermal conductivity of thin samples are flash diffusivity [19] and the comparative method [20]. Flash diffusivity tests require samples between 0.5 and 7 mm thick. The thickness is varied to provide a temperature rise between 40 and 200 ms. Determining the thermal conductivity of a sample from its thermal diffusivity measurement requires knowledge of the sample's heat capacity. This can either be calculated from the known values of the constituents of the composite or measured, for instance, in a differential scanning calorimeter (DSC). The small number of unit cells, perhaps less than one, involved in the small sample size of the DSC, and the small spot size of the laser heat pulse in the diffusivity measurement can introduce significant errors in the measurement of composites.

The comparative method was chosen for the experiments reported here. A composite sample is placed between two reference materials, normally titanium, Armco iron, stainless steel, or Pyroceram, whichever has thermal conductivity approximately equal to or slightly greater than that of the sample. Applying heat to one end of the reference/sample stack generates temperature differentials measured by thermocouples at each end of each reference and at each end of the sample. A linear thermal gradient is assumed to exist along the reference/sample stack, and this assumed thermal gradient is applied to an insulating layer that surrounds the stack. The measurement accuracy of the system is limited by the accuracy of the thermocouples with respect to the temperature differential generated across the sample. To maintain accuracy to  $\pm 5\%$ , the guidelines for sample thickness are 2.5 mm thick for a sample thermal conductivity less than 5 W/m K, 25 mm for 5–50, and 50 mm for 50–200.

#### B. Test Setup

Personnel at the Center for Composite Materials (CCM) at the University of Delaware constructed a guarded heat flow meter, according to American Society for Testing and Materials E1225–04 to provide measurements of circular samples with a diameter of 51 mm. The design was modified due to the small thickness of the composite sample (5 mm), which does not allow the attachment of thermistors, resistance temperature detectors, or thermocouples to the sample. Four thermistors measured the temperature at the meter bars generated by heat from a cartridge heater in the top meter bar, as shown in Fig. 3.

Assuming steady heat flux with a well-insulated system, the heat flux through the temperature measurements  $T_2$  and  $T_5$  is equal to the heat fluxes through the top and bottom meter bars as described in Eq. (3), where  $q$  represents the respective heat flows,  $k_{\text{meter bar}}$  is the thermal conductivity of the meter bar material (stainless steel,

16.2 W/m K), and  $H_{\text{meter bar}}$  represents the respective heights of the meter bars.

The heat flux through the temperature measurements  $T_2$  and  $T_5$  can also be described by the following equations:

$$q_{\text{measure}} = q_{\text{top}} = -k_{\text{meter bar}} \frac{T_2 - T_1}{H_{\text{meter bar top}}} = q_{\text{bottom}} = -k_{\text{meter bar}} \frac{T_6 - T_5}{H_{\text{meter bar bottom}}} \quad (3)$$

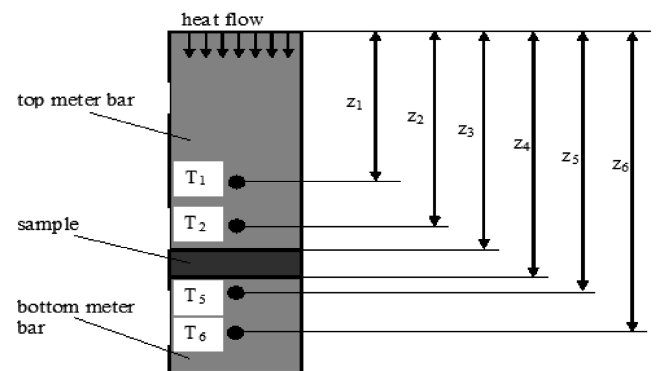
$$q''_{\text{measure}} = -k^*(T_5 - T_2) \quad (4)$$

where  $k^*$  is the serial connection thermal conductivity determined from the thermal conductivities of the meter bars, the sample, and the thermal resistances of the interfaces  $R_{\text{int}}$ , where  $k_{\text{sample}}$  and  $h_{\text{sample}}$  represent the thermal conductivity and the height (thickness) of the sample, respectively:

$$k^* = \left( \frac{H_{\text{meter bar top}}}{k_{\text{meter bar}}} + \frac{h_{\text{sample}}}{k_{\text{sample}}} + \frac{H_{\text{meter bar bottom}}}{k_{\text{meter bar}}} + R_{\text{int}} \right)^{-1} \quad (5)$$

The following equations can be used to determine the through-thickness thermal conductivity of the samples considering the temperatures between  $T_1$  and  $T_5$  (top) or between  $T_2$  and  $T_6$  (bottom), respectively:

$$k_{\text{sample top}} = k_{\text{meter bar}} \frac{(T_2 - T_1)h_{\text{sample}}}{(T_5 - T_2)\Delta z - 2(T_2 - T_1)\Delta z - k_s(T_2 - T_1)R_{\text{int}}} \quad (6)$$

**Fig. 3** Position of thermistor reading locations  $T_1$ – $T_4$  and sample.

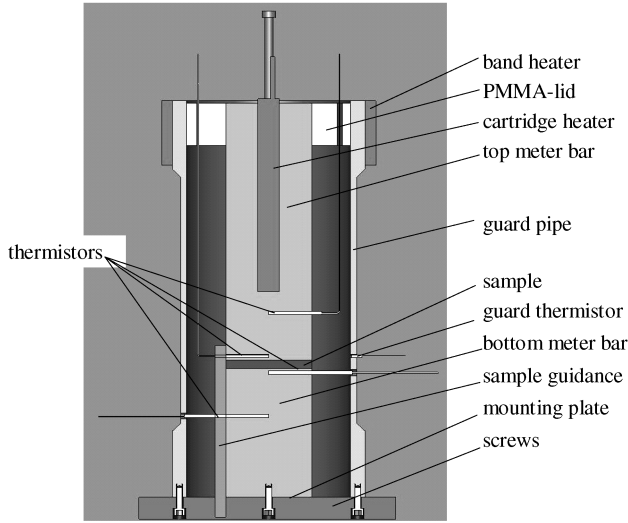


Fig. 4 Through-thickness thermal conductivity test setup.

$$k_{\text{sample bottom}} = k_{\text{meter bar}} \frac{(T_6 - T_5)h_{\text{sample}}}{(T_5 - T_2)\Delta z - 2(T_6 - T_5)\Delta z - k_s(T_6 - T_5)R_{\text{int}}} \quad (7)$$

The reported results average the values derived from both equations. Also, in the test setup, the distances between  $z_2$  and  $z_1$  and between  $z_6$  and  $z_5$  are equivalent and denoted as the term  $\Delta z$ .

Figure 4 shows both a schematic and an image of the test device constructed at CCM. A stainless steel top meter bar is attached to a circular polymethyl methacrylate (PMMA) lid allowing visual affirmation of the proper sitting of the sample during measurement. A cartridge heater at the top of the device was powered with 15 V and 0.52 A to produce a maximum heating power of 7 W and provide an approximate temperature change of 50°C. The samples were attached to the top and bottom bar with a slight layer of high conductive paste (OT-201 from Omega with  $K = 2.3 \text{ W/mK}$ ) applied at the interfaces. The coating of each surface with this paste was done carefully with a reproducible thickness. During the measurements, the thickness of conductive paste layer is assumed to be the same as in the reference measurement. The entire device was placed on a cooling plate kept at 20°C to ensure proper heat flow. A band heater in the guarding pipe generated a linear temperature gradient along the pipe between the heater temperature at the top and the cooling plate temperature at the bottom. The guarding pipe temperature was measured in the region of the sample using a thermocouple. Measurements performed on steel and stainless steel samples with a thickness of 1 in. and on a polyimide (Vespel) sample with a thickness of 0.24 in. proved the accuracy to be within  $\pm 6\%$  of the National Institute of Standards and Technology (NIST) reference data.

#### IV. Thermal Modeling and Verification

##### A. Thermal Modeling

A series of finite element (FE) studies were conducted to investigate the effects of various interface parameters on the through-thickness thermal conductivity of samples arranged in the comparative thermal conductivity test setup described in the last section. To simplify the models, yet capture the essential elements of the through-thickness fiber reinforcement, the studies considered composites of copper rods aligned through the thickness of polymer disks, as is shown in Fig. 5.

The base geometry for all of the simulations consisted of 51-mm-diam, 12-mm-thick samples composed of copper rods in a polytetrafluoroethylene (PTFE) matrix that were held in contact with a stainless steel meter bar. For all simulations, the thermal resistance

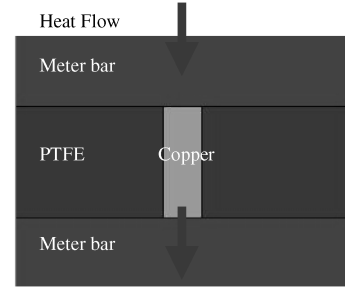


Fig. 5 Diagram of modeling scheme for simple copper rod/polymer disk model.

of the thermal paste is assumed to be  $R_{\text{int}} = 0.000285 \text{ Km}^2/\text{W}$  and the thermal conductivity of the components are  $k_{\text{copper}} = 401 \text{ W/mK}$ ,  $k_{\text{PTFE}} = 0.669 \text{ W/mK}$ , and  $k_{\text{steel}} = 16.2 \text{ W/mK}$ , respectively.

The simulations investigate the concept that the amount of heat that flows through each path will depend on the relative thermal conductivities of the “matrix” composite, the contacting material, and the through-thickness fiber, as well as on the distance between the fibers and the thickness of the part. The following were varied in a series of simulations: 1) the volume fraction of the copper, 2) the thermal conductivity of the meter bar (or other contacting material), 3) the distance between the thermal paths (increase in contacts per area), 4) the thickness of the composite, and 5) the thermal conductivity of the thermal paths themselves.

##### 1. Effect of Volume Fraction

To observe the effect of copper volume fraction on the thermal conductivity of the sample, five samples were simulated. In the simulations, the diameters of a single copper rod in the PTFE matrix were 2.54, 1.9, 1.27, 0.635, and 0.3175 cm. For verification tests of the model, one pure PTFE sample and one pure copper sample were also simulated. Figure 6 illustrates the four of the PTFE/copper samples used in simulation.

The simulation results are plotted in Fig. 7. In general, the thermal conductivity of the copper/PTFE sample increases nonlinearly with the volume fraction of copper and is significantly lower than that from the rule of mixtures, even at high copper volume fraction values. The verification of the model for the pure copper sample agrees well with the input value, within 1.6% of the assumed copper value.

##### 2. Effect of Distance Between Thermal Paths

The separation into a number of discrete thermal paths, its heterogenation, through the high conductivity thermal paths in the

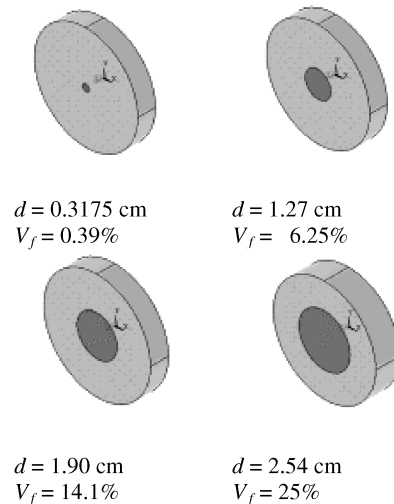


Fig. 6 PTFE/copper samples with one copper string.

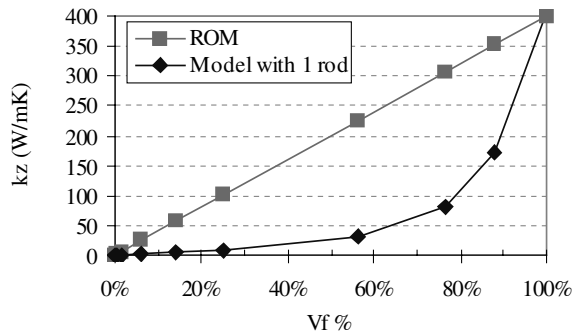


Fig. 7 Effect of copper  $V_f$  on the thermal conductivity of the copper/PTFE sample.

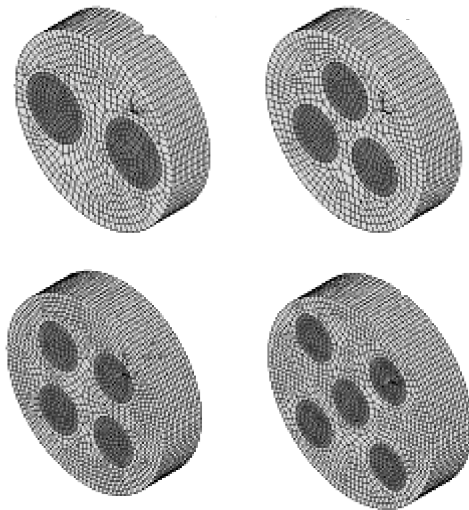


Fig. 8 Copper/PTFE samples with  $V_f = 25\%$ , distributed as 1, 2, 3, 4, and 5 rods.

composite should improve as the distance between thermal paths decreases and the composite more closely resembles an homogeneous structure. Thus, as the number of paths within an area increases at a fixed  $V_{fz}$  of the thermal paths, the thermal conductivity should increase as well.

The FE simulations considered the effect of the number of thermal paths in two ways. In the first set of simulations, comparisons of copper polymer disks with constant  $V_f$ , but with increasing number of copper rods, were conducted at two fiber volume fractions, 6.25 and 25% and with one to five copper rods. Figure 8 shows the pattern in which the copper rods were arranged. The centers for the four-rod configuration are at the midpoints of perpendicular radii, so that the nearest rod is 17.9 mm from another. The centers of the five-rod configuration are at the center and at the two-thirds-point of perpendicular radii, so that the nearest rods are 12.7 mm apart, and the next nearest rods are 24 mm apart.

Table 2 compares the results for  $V_f = 6.25\%$  to the results for  $V_f = 25\%$  with thermal paste assumed between the meter bar and the samples, as well as results for  $V_f = 25\%$  with perfect contact ( $R_{int} = 0$ ) assumed. For all simulation conditions, the thermal conductivity increases as the number of rods increase. With five rods, the thermal conductivity of the sample with  $V_f = 6.25\%$  increased by 25% over its thermal conductivity with a single rod. The results for  $V_f = 25\%$  with thermal paste were similar, showing a 30% increase with five rods over the single-rod simulation condition.

The level of improvement was more pronounced under the assumption of perfect contact. This could have been expected because perfect contact would further reduce the resistance between thermal paths. Although, for the  $V_f = 25\%$  case, simulation results with a single rod obtained for the perfect contact condition were the same as those for the condition with thermal paste, the results for five rods for the perfect contact were 36% higher than those in which thermal paste was assumed.

The second set of FE simulations considered the effect of the number of thermal paths on the modeled unit cell of a copper rod/matrix composite material. The dimensions of the unit cell were varied, while retaining a constant fiber volume fraction. The widths of the fiber  $d_f$  and the unit cell  $d_u$ , described in Fig. 9a, were changed to observe the effect of fiber distribution on the thermal conductivity while keeping constant fiber volume fraction.

Unit cells of varying dimensions, but constant copper volume fraction, that were used for finite element analysis are shown in Figs. 9b and 9c. The volume fraction in all simulations was 25% and the thickness of the samples was 12 mm. Because the unit cell of a 3-D orthogonal fiber architecture has a Z spacing equivalent to the fill yarn spacing, measured in picks per inch (ppi), the simulation results in Table 3 include both a listing of the input unit cell dimensions and a calculation of the fill yarn spacing (ppi) at each unit cell dimension. The results show that, at the finest structure, smallest unit cell dimensions, and highest ppi, the thermal conductivity approaches the prediction from a parallel circuit analysis (rule of mixtures). For the coarser structures, the thermal conductivity falls to a fraction of the ROM estimate.

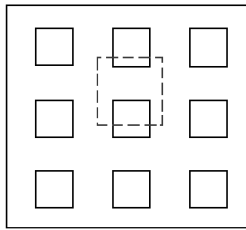
### 3. Effect of Contacting Material (Meter Bar)

To gain a better understanding of the effect of the material contacting the sample, five different metals were considered as the meter bars, again for the case of a single rod in PTFE, and with two total volume fractions,  $V_f = 6.25\%$  and  $V_f = 25\%$ . The results are presented in Fig. 10. For the  $V_f = 25\%$  condition, simulations were conducted both with the assumption of thermal paste and of perfect contact between the meter bars and the sample.

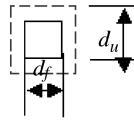
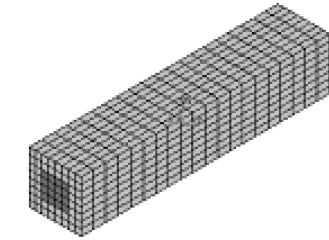
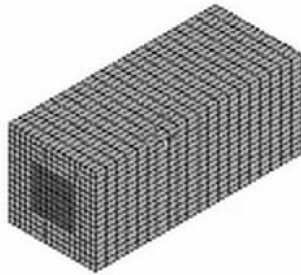
With the thermal paste assumed between the sample and the meter bar, the effect of the thermal conductivity of the meter bar diminishes as its conductivity increases. Significant increases occur in the through-thickness thermal conductivity as the meter bar thermal conductivity rises from 16.2 to 110 W/mK and smaller percentage increases occur as the meter bar thermal conductivity rises beyond 110 W/mK. With perfect contact assumed, the influence of the meter bar thermal conductivity is more pronounced, although the rate of increase in through-thickness thermal conductivity again lessens as the thermal conductivity of the meter bar rises beyond 110 W/mK.

Table 2 Effect of copper distribution on the thermal conductivity of copper/PTFE sample at  $V_f = 6.25$  and 25%

Number of copper rods	$V_f = 6.25\%$	$V_f = 25\%$	
	Sample thermal conductivity (thermal paste), W/mK	Sample thermal conductivity (thermal paste), W/mK	Sample thermal conductivity (perfect contact), W/mK
1	2.5	8.2	8.2
2	2.7	8.7	9.5
3	2.8	9.5	11.1
4	2.9	10.1	13.1
5	3.0	10.6	14.5



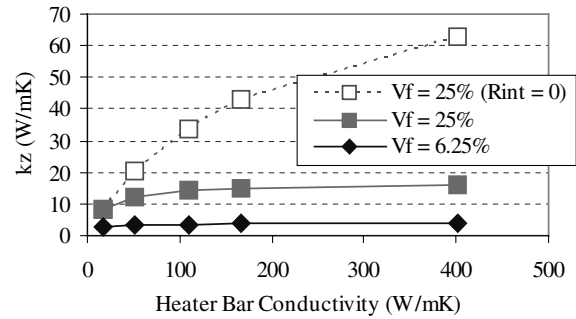
a) Schematic of Unit Cell

b)  $d_f = 1.25$  mmc)  $d_f = 2.5$  mm

**Fig. 9** Schematic of unit cell for FE thermal model and diagrams for two unit cells at  $V_f = 25\%$  with varying fiber dimension, both with length = 12 mm.

#### 4. Effect of Thermal Path Conductivity

By varying the thermal conductivity of the rods from 50 to 800 W/mK, the effect of conductivity of the thermal path on the through-thickness thermal conductivity of the composite was investigated. Again, the configuration of a single rod embedded in a PTFE matrix was simulated at two total volume fractions,  $V_f = 6.25\%$  and  $V_f = 25\%$ . For the  $V_f = 25\%$  condition, simulations were conducted both with thermal paste and with perfect contact. The results are presented in Table 4. Surprisingly, for these samples with 12 mm thickness, the through-thickness conductivity was not sensitive to the increases in the conductivity of thermal paths above a threshold around 200 W/mK.



**Fig. 10** Effect of heat bar material on the thermal conductivity.

#### 5. Effect of Sample Thickness

Several sample thicknesses were simulated, again with one copper rod in PTFE and with thermal paste between the sample and the meter bars. The basis for the previous analyses was a thickness of 12 mm, and this set of simulations varied the thickness from 10 to 500 mm. The results, presented in Fig. 11, show the powerful effect that the sample thickness has on the simulated sample conductivity, with order of magnitude, thermal conductivity increases as the thickness increases.

#### 6. Conclusions from Modeling Results

Many of the interface effects are interdependent, thus each effect cannot be isolated with respect to its ability to influence the thermal conductivity. The thermal conductivity of the meter bar material can raise the modeled thermal conductivity of the sample by an order of magnitude with perfect contact assumed, yet only by a factor of 2 when thermal paste is assumed between the meter bar and the sample. If perfect contact is assumed, the modeled thermal conductivity of the sample approaches ROM as the distance between the contact points falls below 1 mm. When thermal paste is assumed between the sample and the meter bar, and larger distances between contacts are considered, the effect is much smaller.

In general, the most effective mechanisms to increase the thermal conductivity are those that reduce the resistance between the thermal paths, namely, increasing the contacting material conductivity, reducing the distance between thermal paths, and lowering the contact resistance between the sample and the meter bar. As the samples become thicker, the relative effect of the interface diminishes and the materials approach the thermal conductivity expected by a parallel circuit analysis (ROM).

#### B. Experimental Verification of Copper/Polytetrafluoroethylene Thermal Conductivity Model

To verify the modeling efforts, a matrix of Teflon disks was fabricated with copper rods aligned through the thickness. The number of rods varied between one and four, and the volume fraction of the rods varied from 0.8 to 19.5%. A total of 35, 51-mm-diam Teflon (PTFE) samples were machined and solid copper rods inserted, as diagrammed in Fig. 12. One additional sample evaluated the Teflon thermal conductivity with no copper content. After machining, the samples were ground and polished to provide a smooth surface.

**Table 3** Effect of reinforcement distribution, unit cell analysis (copper,  $V_f = 25\%$ , perfect contact)

Fiber width $d_f$ , mm	Unit cell width $d_u$ , mm	Equivalent DPI $\times$ DPI in 3-D weave	Thermal conductivity, W/mK
0.078125	0.15625	$163 \times 163$	100
0.15625	0.3125	$81 \times 81$	98
0.3125	0.625	$41 \times 41$	92
0.625	1.25	$20 \times 20$	83
1.25	2.5	$10 \times 10$	69

Table 4 Effect of thermal path conductivity, single rod in PTFE

Reinforcement thermal conductivity, W/mK	$V_f = 6.25\%$		$V_f = 25\%$	
	Sample thermal conductivity (thermal paste), W/mK		Sample thermal conductivity (perfect contact), W/mK	
50	1.9		5.6	
100	2.2		6.8	
200	2.4		7.7	
400	2.5		8.2	
800	2.6		8.5	

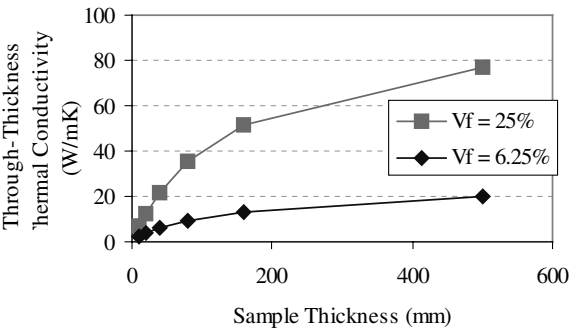


Fig. 11 Effect of sample thickness on the thermal.

Figure 13 groups the copper/PTFE thermal conductivity results by the number of rods, then compares them to the FE simulation results. The test results broadly agree with the FE models, despite the scatter in the data, with most points falling in a band between the FE simulation results for one and four rods. Much of the scatter in the data comes from variation in the thickness of the samples, which was unfortunately not controlled in the sample fabrication. The general trends of increasing through-thickness thermal conductivity with increasing volume fraction and with decreasing distance between the thermal paths, that is, greater number of copper rods, seen in the modeling data were also seen in the test data.

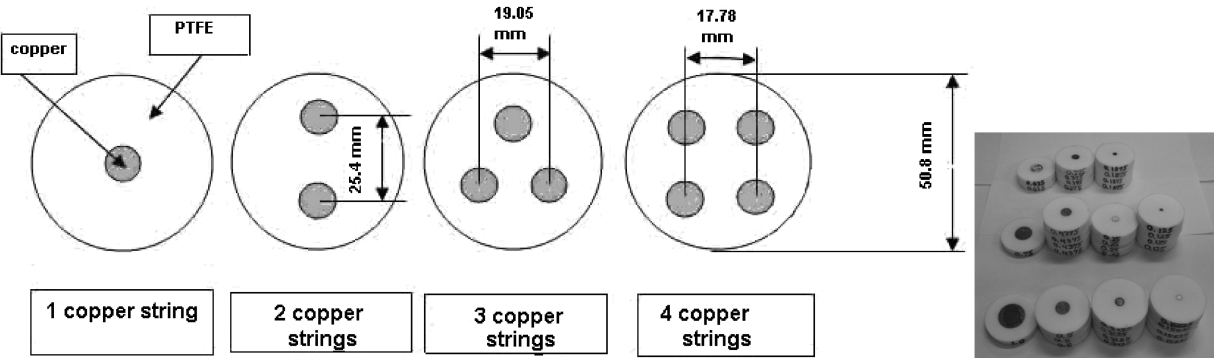


Fig. 12 Schematic and image of copper rod/Teflon samples for model verification matrix.

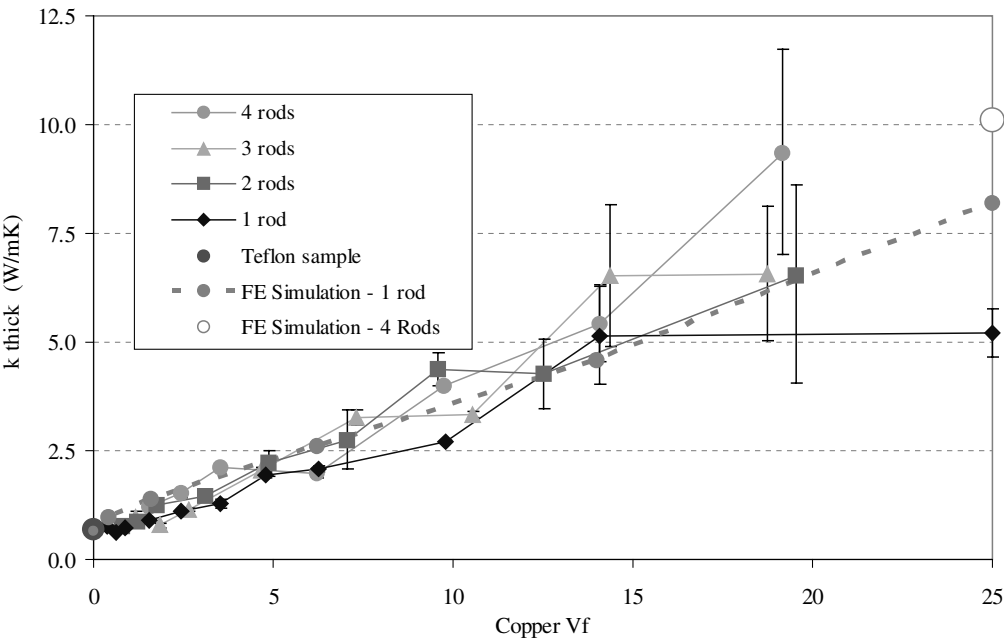


Fig. 13 Copper/PTFE thermal conductivity test data.

## V. Thermal Conductivity Measurements of Test Matrix of Three-Dimensional Composites

### A. Preform and Composite Test Specimen Descriptions

A test matrix of composites based on 3-D orthogonally woven preforms were fabricated and their through-thickness thermal conductivity tested. Two series of 3-D orthogonally woven preforms at Z direction volume fraction contents of 1.8, 3.7, and 5.5% were manufactured by 3TEX; one with GranocYS-80 6k yarns in the Z direction and a second with 10-ply, 34-gauge soft annealed copper wires in the Z direction. The trials also included variations in the fill and warp fiber types to investigate possible effects of in-plane thermal conductivity on the out-of-plane thermal conductivity measurements. The spacing of the Z yarn thermal paths was approximately constant and set by the eight yarns per inch (dpi) reed and by five fill yarn insertions per inch spacing (ppi) for an areal density of 40 thermal paths per square inch (6.2/cm<sup>2</sup>).






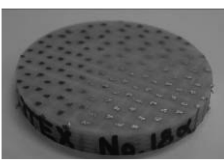
The approximately 12-mm-thick preforms were infused with epoxy ( $k_{\text{resin}} = 0.19$  W/mK) using vacuum assisted resin transfer

molding techniques, then the resultant composites were machined into 51-mm-diam samples and ground parallel and flat. A slight layer of high-conductive paste (OT-201 from Omega, with  $K = 2.3$  W/mK) applied at the interfaces attached the samples to the top and bottom meter bars in the test setup. Again, the interfacial resistance  $R_{\text{int}}$  of  $5.5 \times 10^{-4}$  (K · m<sup>2</sup>)/W, which had been determined by the testing with NIST standards, was used in the thermal conductivity calculations. Each reported result consists of the average of two measurements for each sample. The samples were also sent to Graftech, a division of UCAR in Cleveland, Ohio, to verify the results with an independent set of tests.

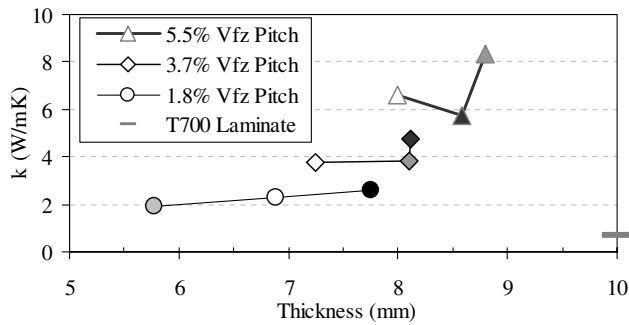
### B. Three-Dimensional Composite Through-Thickness Thermal Conductivity Test Results

Table 5 describes the preforms, lists the composite thicknesses, and shows the measurements of through-thickness thermal conductivity by CCM, as well as those measured by Graftech. An outlying test point (copper  $V_{fz} = 5.5\%$  with E-glass in fill and warp)

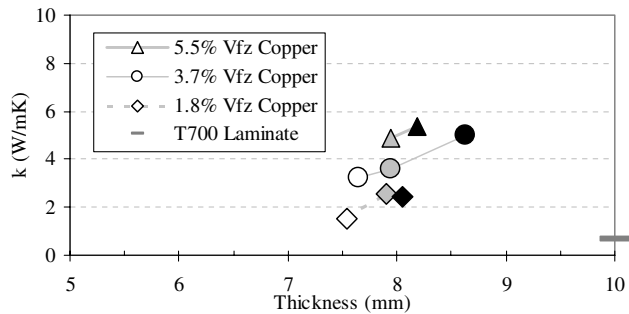
**Table 5** Test matrix of through-thickness thermal conductivity measurements of 3-D woven composites

	Z	Fill	Warp	Sample thickness, mm	CCM $k_z$ , W/mK	Graftech $k_z$ , W/mK	
1	YS80 1.8% (pitch)	CN80 18.9% (pitch)	T700 18.8% (PAN carbon)	7.8	2.6	2.5	
2	YS80 3.7% (pitch)	CN80 18.0% (pitch)	T700 14.1% (PAN carbon)	8.1	4.7	4.8	
3	YS80 5.5% (pitch)	CN80 13.8% (pitch)	T700 10.8% (PAN carbon)	8.6	5.8	7.6	
7	YS80 1.8% (pitch)	AS3 19.0% (PAN carbon)	T700 19.1% (PAN carbon)	5.8	1.9	3	
8	YS80 3.7% (pitch)	AS3 17.8% (PAN carbon)	T700 14.2% (PAN carbon)	8.1	3.8	5.7	
9	YS80 5.5% (pitch)	AS3 13.0% (PAN carbon)	T700 10.4% (PAN carbon)	8.8	8.3	4.6	
13	YS80 1.8% (pitch)	E-glass 19.3%	E-glass 19.3%	6.9	2.3	1.6	
14	YS80 3.7% (pitch)	E-glass 18.4%	E-glass 15.2%	7.2	3.8	4.3	
15	YS80 5.5% (pitch)	E-glass 14.8%	E-glass 12.2%	8.0	6.6	7.4	
4	Copper 1.8%	CN80 25.8% (pitch)	T700 20.3% (PAN carbon)	8.1	2.4	2.8	
5	Copper 3.7%	CN80 23.0% (pitch)	T700 18.1% (PAN carbon)	8.6	5.0	5.1	
6	Copper 5.5%	CN80 19.1% (pitch)	T700 15.5% (PAN carbon)	8.2	5.4	4.4	
10	Copper 1.8%	AS3 26.1% (PAN carbon)	T700 20.8% (PAN carbon)	7.9	2.6	2.9	
11	Copper 3.7%	AS3 21.0% (PAN carbon)	T700 16.8% (PAN carbon)	8.0	3.6	4.1	
12	Copper 5.5%	AS3 21.1% (PAN carbon)	T700 16.7% (PAN carbon)	8.0	4.9	5.2	
16	Copper 1.8%	E-glass 19.3%	E-glass 19.3%	7.5	1.5	2.4	
17	Copper 3.7%	E-glass 18.4%	E-glass 15.2%	7.7	3.3	3.7	
18	Copper 5.5%	E-glass 14.8%	E-glass 12.2%	6.2	<b>1.9</b>	<b>0.7</b>	
19	0% Laminate	T700 25% (PAN carbon)	T700 25% (PAN carbon)	1.47	0.7		





a) YS-80 pitch yarns in Z



b) Plied copper wires in Z

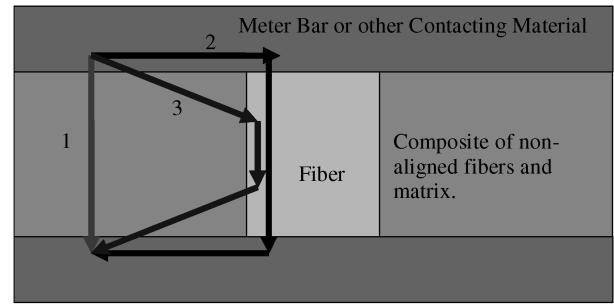
**Fig. 14** Measured through-thickness thermal conductivity for composites based on 3-D woven preforms with varying fiber volume fractions in Z. (White points represent composites with E-glass in warp and fill. Gray points represent composites with polyacrylonitrile (PAN) carbon in warp and fill. Black points represent composites with PAN carbon in the warp and YS95 pitch carbon in the fill.)

is highlighted in bold font. On average, the test data of Graftech and of CCM agreed within around 20%.

The data show that, with as little as 1.8% Z yarn fiber content  $V_{fz}$  of Granoc YS-80 pitch yarns, the composites based on 3-D woven preforms demonstrated 2–3 times the measured thermal conductivity over the 2-D laminate. With 5.5%  $V_{fz}$ , the measured thermal conductivity was as much as 12 times greater. Slightly lower thermal conductivity results were achieved with the plied copper wire in the Z direction, reaching a maximum of approximately 8 times greater than that of the laminate. Figures 14a and 14b plot the measured through-thickness thermal conductivity values versus sample thickness, with the various warp and fill directional fibers.

Two of the basic trends from the modeling and the copper rod/PTFE tests are confirmed: 1) the measured through-thickness thermal conductivity increases with increased Z fiber volume fraction, and 2) there is a correlation of increased thermal conductivity with increased thickness. Another trend identified in the modeling was confirmed by the test data: an increase in the areal density of thermal paths (contact points/cm<sup>2</sup>) increases the measured thermal conductivity.

Table 6 compares data from the copper rod/PTFE and 3-D preform matrix tests that most closely approximate the FE model results for a single copper rod at the minimum thickness modeled. There is excellent agreement between the model and the most closely related



**Fig. 15** Schematic of available thermal pathways.

copper/PTFE test point, the single rod at  $V_f = 6.25\%$ . The remaining copper/PTFE specimens were thinner and had lower copper volume fractions, both of which were shown in the modeling to lower the thermal conductivity. However, because these specimens had more contact points, tests on them yielded thermal conductivities approximately equal to the single rod model prediction. The test results for the composites based on 3-D preforms provide further evidence of the influence of distance between the thermal paths. The 40 contacts/in<sup>2</sup> available with the 3-D preforms represent a large increase in areal density of thermal paths and, correspondingly, their measured thermal conductivities were significantly greater than those of the copper/PTFE samples, despite having thinner specimens with lower volume fractions of conductive paths.

There are several other observations about the data:

1) Despite the higher thermal conductivity of the copper, the samples with copper in the Z measured consistently lower through-thickness thermal conductivity than those with the YS80 pitch yarns.

2) For the samples with pitch carbon in the Z yarn position, the relation was not consistent between the in-plane fibers used and through-thickness thermal conductivity obtained.

3) For the samples with copper in the Z yarn position, the thermal conductivity increased as the thermal conductivity of the in-plane yarns increased.

The explanation for this last set of observations may lie in the effects of the thinness of the samples and the limited number of thermal pathways available. Figure 15 shows a unit cell and the thermal pathways from a point in the top meter bar at some distance from the through-thickness yarn to an opposing point in the bottom meter bar. Three basic paths are possible: 1) directly through the matrix, 2) along the meter bar to the nearest fiber, then back along the meter bar, and 3) through the matrix to the nearest fiber, then back through the matrix.

The amount of heat that flows through each path will depend on the relative thermal conductivities of the in-plane fiber matrix, the contacting material, and the through-thickness fiber, as well as on the distance between the fibers and the thickness of the part. It will also depend on the thermal resistance between the matrix and the through-thickness fiber. This coarse model may help to explain the lower through-thickness thermal conductivity of the samples with copper in the Z. The pitch carbon fibers are highly anisotropic, with high thermal conductivity along the fiber axis and around 1 W/mK in the radial direction. Because of the isotropic nature of the copper wires, less resistance to heat flow into the matrix near the Z positions exists and a larger portion of the heat flows through the lower in-plane fiber/resin matrix.

**Table 6** Comparison of model, copper/PTFE, and 3-D preform matrix test results

Source	Thickness, mm	Copper $V_f$ , %	Contact points/cm <sup>2</sup>	$k_z$ , W/mK
Model (copper)	10.0	6.25	0.05 (1 rod)	2.2
Copper/PTFE test #15	9.4	6.25	0.05 (1 rod)	2.1
Copper/PTFE test #17	9.1	4.9	0.1 (2 rods)	2.2
Copper/PTFE test #19	9.0	4.8	0.15 (3 rods)	2.0
3-D Preform #3 (copper)	8.2	5.5	6.2 (8 dpi × 5 ppi)	5.8
3-D Preform #9 (YS80)	8.8	5.5	6.2 (8 dpi × 5 ppi)	8.3

**Table 7 Through-thickness thermal conductivity of plated 3-D preform composites**

No.	Z	Fill	Warp	Height, mm	Unplated $k_z$ , W/mK	Plated $k_z$ , W/mK	ROM $k_z$ , W/mK
3	YS80 5.5% (pitch)	CN80 13.8% (pitch)	T700 10.8% (PAN carbon)	8.6	5.8	11.6	17.6
15	YS80 5.5% (pitch)	E-glass 14.8%	E-glass 12.2%	8.0	6.6	10.6	17.6
6	Copper 5.5%	CN80 19.1% (pitch)	T700 15.5% (PAN carbon)	8.2	5.4	9.9	21.9
12	Copper 5.5%	AS3 21.1% (PAN carbon)	T700 16.7% (PAN carbon)	8.0	4.9	7.8	21.9
4	Copper 1.8%	CN80 25.8% (pitch)	T700 20.3% (PAN carbon)	8.1	2.4	12	7.2
18	Copper 5.5%	E-glass 14.8%	E-glass 12.2%	6.2	<b>1.9</b>	5.8	21.9

### C. Three-Dimensional Composite Through-Thickness Thermal Conductivity Test Results: Plated Specimens

Six of the test samples tested were chemically etched and plated with copper, then retested. When placed in the test setup, the copper plating increases the effective thermal conductivity of the contacting material by providing a highly conductive interface between the meter bar with thermal paste and the sample. The modeling shows that this would increase the measured thermal conductivity of the samples. The test results in Table 7 confirm the modeling predictions, with the plated specimens exhibiting a nearly twofold increase in measured thermal conductivity. The bottom two points in the table merit suspicion: the copper 1.8%  $V_f$  copper exhibited higher conductivity than even ROM would suggest, and the E-glass with copper specimen had been an outlier point in previous testing.

## VI. Conclusions

The through-thickness thermal conductivity of composites based on 3-D orthogonal woven hybrid fabrics, with highly thermally conductive yarns woven into the through-thickness Z direction, greatly exceed that of laminate uniaxial or biaxial composites. Tests of unoptimized 3-D composites with pitch carbon yarns in the Z demonstrated through-thickness thermal conductivity as high as 8.3 W/mK, on the order of some metals, for example, titanium Navy alloy\*\* at 7.5 W/mK and stainless steel 304 [21] at 16.3 W/mK. Tests on an equivalent T700 carbon epoxy laminate measured only 0.7 W/mK, an order of magnitude lower.

Thermal modeling results showed that, due to the heterogeneous character of the composites based on 3-D woven preforms, the measured thermal conductivity and the thermal behavior of such composites depends on the elements of the thermal system in which they are placed, because the system has a role in distributing the homogeneous heat flow into the composite. This was further evidenced by experiments in which plating the composite surfaces increased the thermal conductivity by approximately 2 times.

Thus, the through-thickness thermal conductivity exhibited by composites based on 3-D orthogonal woven preforms will be a function of several elements: 1) thermal conductivity of the material in contact with the composite, 2) thickness of the composite, 3) volume fraction of Z yarns in the composite, 4) areal density of Z yarns in the composite, 5) isotropy of the Z yarns in the composite, and 6) thermal conductivity of Z yarns in the composite, if the conductivity is below a threshold of around 100–200 W/mK.

Further increases in through-thickness thermal conductivity for the composites based on 3-D woven preforms are possible. Optimization of the 3-D woven fiber architectures to increase the areal density of thermal paths (Z yarns per area) would increase the measured thermal conductivity beyond the maximum of 8.3 W/mK achieved in the test matrix of 3-D composites.

## Acknowledgments

The work described was conducted as part of United States Air Force Small Business Innovative Research contract FA8650-06-C-3616. The authors would like to acknowledge Edwin Forster of The Air Force Research Laboratory for his help and guidance. The

authors would also like to acknowledge Olivia Polczyk for her diligent work in the thermal conductivity testing.

## References

- [1] Springer, G. S., and Tsai, S. W., "Thermal Conductivities of Unidirectional Materials," *Journal of Composite Materials*, Vol. 1, No. 2, 1967, pp. 166–173.  
doi:10.1177/002199836700100206
- [2] Behrens, E., "Thermal Conductivities of Composite Materials," *Journal of Composite Materials*, Vol. 2, No. 1, 1968, pp. 2–17.
- [3] Thornburg, J. D., and Pears, C. D., "Prediction of the Thermal Conductivity of Filled and Reinforced Plastics," American Society of Mechanical Engineers Paper 65-WA/HT-4, 1965.
- [4] Farmer, J. D., and Covert, E. E., "Thermal Conductivity of a Thermosetting Advanced Composite During Its Cure," *Journal of Thermophysics and Heat Transfer*, Vol. 10, No. 3, July–Sept. 1996, pp. 467–475.  
doi:10.2514/3.812
- [5] Hashin, Z., "Analysis of Composite Materials: A Survey," *Journal of Applied Mechanics*, Vol. 50 No. 9, 1983, pp. 481–505
- [6] Hatta, H., and Taya, M., "Thermal Conductivity of Coated Filler Composites," *Journal of Applied Physics*, Vol. 59, No. 6, 1986, pp. 1851–1860.  
doi:10.1063/1.336412
- [7] Chawla, K. K., *Composite Materials, Science and Engineering*, Springer–Verlag, New York, 1987.
- [8] Hasselman, D. P. H., Donaldson, K. Y., and Thomas, J. R., Jr., "Effective Thermal Conductivity of Uniaxial Composites with Cylindrically Orthotropic Carbon Fibers and Interfacial Thermal Barrier," *Journal of Composite Materials*, Vol. 27, No. 6, 1993, pp. 637–644.  
doi:10.1177/002199839302700605
- [9] Hasselman, D. P. H., and Johnson, L. F., "Effective Thermal Conductivity of Composites with Interfacial Thermal Barrier Resistance," *Journal of Composite Materials*, Vol. 21, No. 6, 1987, pp. 508–515.  
doi:10.1177/002199838702100602
- [10] Silverman, E. M., "Product Development of Engineered Thermal Composites for Cooling Spacecraft Electronics," *Northrop Grumman Technology Review Journal*, Vol. 13, No. 2, Fall/Winter 2005, pp. 1–19.
- [11] Kiuchi, N., Ozawa, K., Komami, T., Katoh, O., Arai, Y., Watanabe, T., and Iwai, S., "Pitch-Based Carbon Fiber with High Thermal Conductivity for New Advanced Thermal Design," *Proceedings of the 30th International SAMPE Technical Conference*, Society for the Advancement of Material and Process Engineering, Covina, CA, 1998, pp. 68–77.
- [12] Biggs, D. M., "Conductive Polymeric Compositions," *Polymer Engineering and Science*, Vol. 17, No. 12, Dec. 1977, pp. 842–847.  
doi:10.1002/pen.760171206
- [13] Watts, R. J., Kistner, M., Druma, A. M., and Alam, K., "Materials Opportunity for Spacecraft and Aerospace Thermal Management," *Space Technologies and Applications International Forum: STAIF 2005*, edited by M. S. El-Genk, American Inst. of Physics, Melville, NY, 2005, pp. 22–31.
- [14] Mohamed, M. H., Bogdanovich, A. E., Dickinson, L., Singletary, J. N., and Lienhart, R. B., "A New Generation of 3D Woven Fabric Preforms and Composites," *SAMPE Journal*, Vol. 37, No. 3, 2001, pp. 8–17.
- [15] Mohamed, M. H., and Zhang, Z., U.S. Patent 5,085,252, 1992.
- [16] Sharp, K., Bogdanovich, A. E., Schuster, J., and Heider, D., "Through-Thickness Thermal Conductivity in Composites Based on 3-D Fiber Architectures," *SAE 2007 AeroTech Congress*, American Society of Metals, 07ATC-212, 2007.

\*\*\*Ti5Al1Sn1Zr1V0.8Mo Properties and Applications" and "Titanium-Comparison With Other Metals," <http://www.azom.com>.

- [17] Sharp, K. W., Bogdanovich, A. E., Mungalov, D., and Wigent, D., and Mohamed, M. H., "High Modulus Fibers in 3-D Woven and Braided CMC Preforms," *Proceedings of the SAMPE Fall Technical Conference 2005*, Society for the Advancement of Material and Process Engineering, Covina, CA, 2005.
- [18] Ko, F., "Preform Fiber Architecture for Ceramic Matrix Preforms," *Ceramic Bulletin*, Vol. 68, No. 2, 1989, p. 402.
- [19] "Standard Test Method for Thermal Diffusivity of Solids by the Flash Method," American Society for Testing and Materials E1461-01. doi:10.1520/E1461-01
- [20] "Standard Test Method for Thermal Conductivity of Solids by Means of the Guarded-Comparative-Longitudinal Heat Flow Technique," American Society for Testing and Materials E1225-04. doi:10.1520/E1225-04
- [21] Lyman, T (ed.), *Metals Handbook*, 8th ed., Vol. 1, American Society of Metals, Metals Park, OH, 1961.

A. Palazotto  
Associate Editor